Centennial Oscillations in an Ocean–ice Coupled Model

Jin Xiangze (金向泽),

LASG, Institute of Atmospheric Physics, Chinese Academy of Sciences, Beijing 100029

Huang Ruixin (黄瑞新) and Yang Jiayan (杨嘉岩)

Dept. of Physical Oceanography, Woods Hole Oceanographic Institution, Woods Hole, MA 02543

(Received June 8, 1998; revised March 15, 1999)

ABSTRACT

Irregular centennial oscillations, with a spectral peak at 106 years, were obtained from an ocean–ice coupled model for the North Atlantic with realistic coastline and bottom topography. The model's thermohaline circulation is forced by mixed boundary conditions, i.e., a Haney–type relaxation condition for temperature, but an equivalent virtual salt flux condition for salinity. All forcing fields are taken from the observed monthly mean climatological wind stress and buoyancy fluxes.

The oscillations appeared in the form of a surface–intensified tripole in both the sea surface temperature and salinity fields located in the vicinity of the Labrador Sea. The oscillations involve a delicate interplay between heat and fresh water advection by meridional overturning circulation, horizontal gyres, vertical convection, and the seasonal cycle. The oscillations are primarily controlled by the salinity component of the circulation; however, sea ice plays a minor role in driving the oscillations observed in the model. On the other hand, a regular seasonal cycle in the forcing fields is an important ingredient for the centennial oscillations.

Key words: Thermohaline circulation, Ocean model, Oscillation

1. Introduction

Observations indicate that the subpolar North Atlantic Ocean, particularly the Labrador Sea, is a main center where large–amplitude, long–term climate anomalies have ocurred (e.g., Kushnir, 1994; Deser and Blackmon, 1993). Modeling studies using coupled atmosphere–ocean general circulation models also suggest that the Labrador Sea is a major source for interdecadal climate variabilities (e.g., Delworth et al., 1993). Some of these variations are due to the active atmosphere–ocean interaction (e.g., Delworth, 1996), while others appear to be mainly attributable to oceanic processes only (e.g., Delworth et al., 1993).

This paper presents results from a three–dimensional ocean general circulation model which is coupled with an active sea–ice model and uses realistic topography and coastlines. When forced by the monthly mean surface fluxes of momentum, heat, and fresh water, the model produces an oceanic state that resembles observations. Meanwhile the model also generates internal oscillations of centennial or longer periods. The anomaly patterns consist of alternating warming and cooling between the Labrador Sea and a region to its southwest. This is quite similar to the previous modeling results by Delworth et al. (1993). However, the dominant period is considerably longer in our model. Although our model excludes the atmospheric feedbacks, results from our model are in agreement with the conclusion of Delworth et al. that the Labrador Sea oscillations at such long time scales are mainly due to

the internal oceanic processes rather than the active atmopshere–ocean interactions.

The objective of this paper is to describe those anomalies and their driving mechanisms. In addition, we will compare our model results with previous modeling works, and assess their relevance to climate changes in the subpolar North Atlantic Ocean. To do so, we will analyze all processes that affect the density in the deep-water formation regions, i.e., advection by meridional overturning, horizontal gyre, convection, and diffusion, and examine how they interact with each other. Since the model includes the seasonal variation, we will also examine its role, including the possibility of the type of nonlinear subharmonic responses discussed by Yang and Huang (1996). We calculate the time scale of low-latitude response to the Labrador Sea variations and compare it with the recent observational studies by Curry and McCartney (1996). This comparison and subsequent analyses point to some genetic deficiency in ocean GCMs, especially those non-eddy resolving ones, for setting proper pathways away from the water mass formation sites.

This paper is organized in the following order: The model and forcing fields are described in Section 2, model results are then presented in Section 3, the mechanisms for the low-frequency variations are discussed in Section 4, and a summary will be given in section 5.

2. The model

A numerical model for the North Atlantic is set up based on the Modular Ocean Model 2 code (Pacanowsky, 1995) and it is coupled to a thermodynamic sea ice model similar to that of Parkinson and Washington (1979). Because our model does not resolve the meso-scale eddies, the newly developed scheme of isopycnal / dipycnal mixing and meso-scale eddy transport of tracers implemented in the standard code have been used in our experiments. The model domain covers from the Equator to 74°N and from 95°W to 20°E, with the realistic coastline (with the Iceland excluded) and bottom topography. The horizontal resolution is 2.5° by 2.0° in the zonal and meridional directions. There are 20 layers vertically, with layer thickness increasing from 50 m at the surface to 400 m for the deepest layer.

The model is driven by the monthly mean wind stress distribution by Hellerman and Rosenstein (1983). A Haney-type of formula is used as the thermal boundary condition for the model, so the heat flux F_H is determined by

$$F_H = D(T_A - T_S) + Q, \tag{1}$$

where T_A and T_S are the atmospheric equilibrium and oceanic temperature at the sea surface (Haney, 1971). In fact, Eq. (1) represents the linearization of the total heat flux at the equilibrium temperature T_A; D is the first order Taylor expansion coefficient, Q contains the net downward flux of solar radiation across the ocean surface, minus the upward flux of longwave radiation and latent heat from an ocean surface at temperature T_A. Both D and Q are related to all processes that affect the surface heat fluxes, so they vary in space. In this model they are calculated from the ECMWF monthly mean surface air temperature, pressure, specific humidity, wind speed, cloud fraction, and solar radiation (Trenberth, 1992).

The model is first spun up under a restoring boundary condition for salinity, i.e., the surface virtual salt flux is

$$F_S = \frac{\Delta Z_1 (S_{obs} - S_S)}{\tau}, \tag{2}$$

where ΔZ_1 is the thickness of the upper layer, S_{obs} is the monthly-mean climatological

surface salinity (Levitus, 1994), S_S is the sea surface salinity, $\tau = 120$ d is the relaxation time. We have chosen this relaxation time following the suggestion by Tziperman et al. (1994). As the model reaches a quasi-equilibrium state, the equivalent virtual salt flux is diagnosed from the solution. Afterward, the model is restarted from the existing solution and continues to run under the mixed boundary conditions.

When the predicted sea surface temperature cools to near the freezing point of seawater, sea ice appears. Sea ice in the model is simulated by a thermodynamic model based on that of Parkinson and Washington (1979) and a simple sea ice advection scheme. The ocean and ice are coupled through the heat flux and freshwater flux due to ice freezing / melting; however, there is no dynamic interaction between water and ice.

In the ice-covered area, the surface heat flux F_H is controlled by

$$F_H = F_{aw}(1 - A_{leads}) + F_{iw} A_{leads}, \tag{3}$$

where $F_{aw} = D(T_a - T_S) + Q$ is the air-water heat flux, $F_{iw} = k(T_b - T_S)$ is the ice-water heat flux (T_b is the freezing point of sea water, k is a constant parameterizing the turbulent heat flux across the water-ice interface), and A_{leads} registers the percentage of area covered by ice in each grid.

In the vertical direction ice freezing / melting depends on the net heat balance of the sea ice, i.e., the ice-water heat flux F_{iw} minus the air-ice heat flux F_{ai}, where F_{ai} is calculated by the above Haney-type formula. Note that coefficients D and Q used here are different from the ones used for the calculation of F_H because of different surface albedo and latent heat of vaporization.

In the lateral direction, expansion and contraction of ice coverage depend on the surface heat flux F_{aw} and the predicted sea surface temperature (SST). Because of the existence of leads, the wintertime heat loss through ice gaps can drive the SST below the freezing point T_b; thus, ice coverage expands laterally to release energy to maintain the SST at T_b.

When $F_{aw} > 0$, a portion of this energy, $1 - A_{leads}$, will be used for lateral melting of ice and the remaining portion is used to warm sea water.

The change in the surface salinity due to brine rejection is

$$ds = \frac{\bar{S}\delta H_i}{\Delta z_1}, \tag{4}$$

where H_i is defined as the mean thickness of sea ice in one grid.

Sea ice is transported by current, however, there is no interaction between ice and current. A simple upwind scheme is used to transport the ice thickness H_i and ice leads A_{leads}. When $A_{leads} > 98\%$, areas of sea ice can overlap each other; thus, an upper limit of 98% leads is set for the model.

3. The numerical experiments

The model is first spun up under the relaxation conditions for both temperature and salinity. The oceanic model parameters are the following: horizontal and vertical momentum dissipation coefficients are $1.0 \times 10^9 \text{cm}^2\text{s}^{-1}$ and $10\ \text{cm}^2\text{s}^{-1}$, isopycnal and diapycnal mixing coefficients are $2.0 \times 10^7 \text{cm}^2\text{s}^{-1}$ and $0.6\ \text{cm}^2\text{s}^{-1}$. Time steps are 2 d for tracers and 1 h for momentum. After a 6245-year integration, the model reaches a state of quasi-equilibrium with a regular seasonal cycle. The annual mean state is rather similar to the climatology because the relaxation conditions were applied to both the temperature and salinity fields (Fig. 1). The

annual maximum ice coverage, the lightly shaded area in Fig. 1a, resembles observations. The surface salinity has a high value of 37 psu in the middle of the subtropical gyre, low salinity in the subpolar gyre, and a kink south of Greenland. The Gulf Stream system is clearly defined, including its bifurcation into the North Atlantic Current south of Newfoundland. There is a weak and less well-defined southward Eastern Greenland Current. It will be shown below that the spatial patterns of the mean salinity and velocity fields play an important role in setting up the centennial oscillation in the model.

Thermohaline circulation is driven by water mass formation at high latitudes. In this model, the subpolar mode water mass formation is the major contributor to the thermohaline circulation because the other sources of deep water in Norway and Greenland are not fully simulated due to the artificial model boundary at 74°N. Maps of vertical velocity (not included) between 500 and 700 meters depth confirmed that sinking is mostly confined to the region of subpolar mode water formation, i.e., south of Greenland. In fact, the somewhat concentrated sinking region near the site of subpolar mode water formation helps us to understand the thermohaline circulation better.

Using the seasonal forcing, there is clearly a well-defined seasonal cycle in the model. During one annual cycle, the basin-mean surface temperature fluctuates from 17.0°C to 20.8°C, and the basin-mean surface salinity fluctuates between 35.417 and 35.487 psu. The large amplitude of surface temperature is due to the strong annual cycle in surface heat flux; while the relatively small amplitude of surface salinity is due to the annual cycle in the equivalent evaporation / precipitation, including the freshwater flux due to ice freezing / melting.

The application of the relaxation condition to the salinity field is, of course, artificial. Although we have used a relatively long relaxation time, 120 d, for the salinity balance equation, a solution obtained under the relaxation condition is inevitably subject to its intrinsic limitation. One of the most important limitations of the relaxation condition for salinity is that the

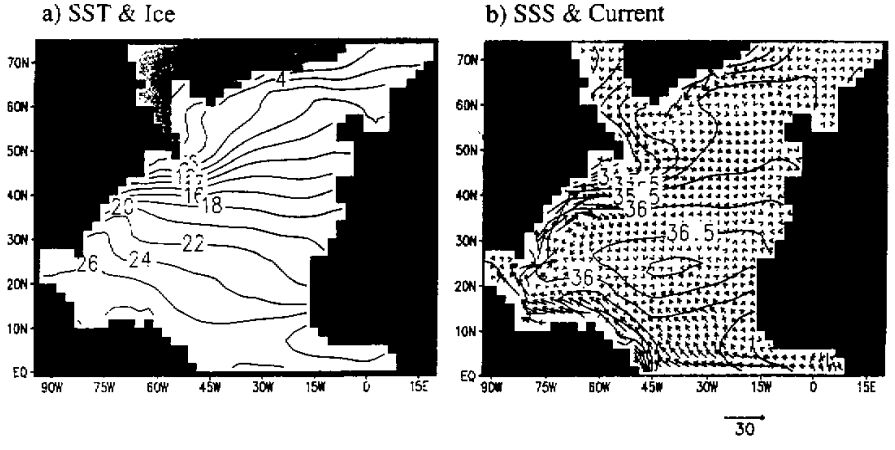

Fig. 1. Annual-mean circulation of the model: (a) surface temperature and ice coverage (the lightly shaded area indicates the area of ice concentration larger than 40%); (b) surface velocity and surface salinity.

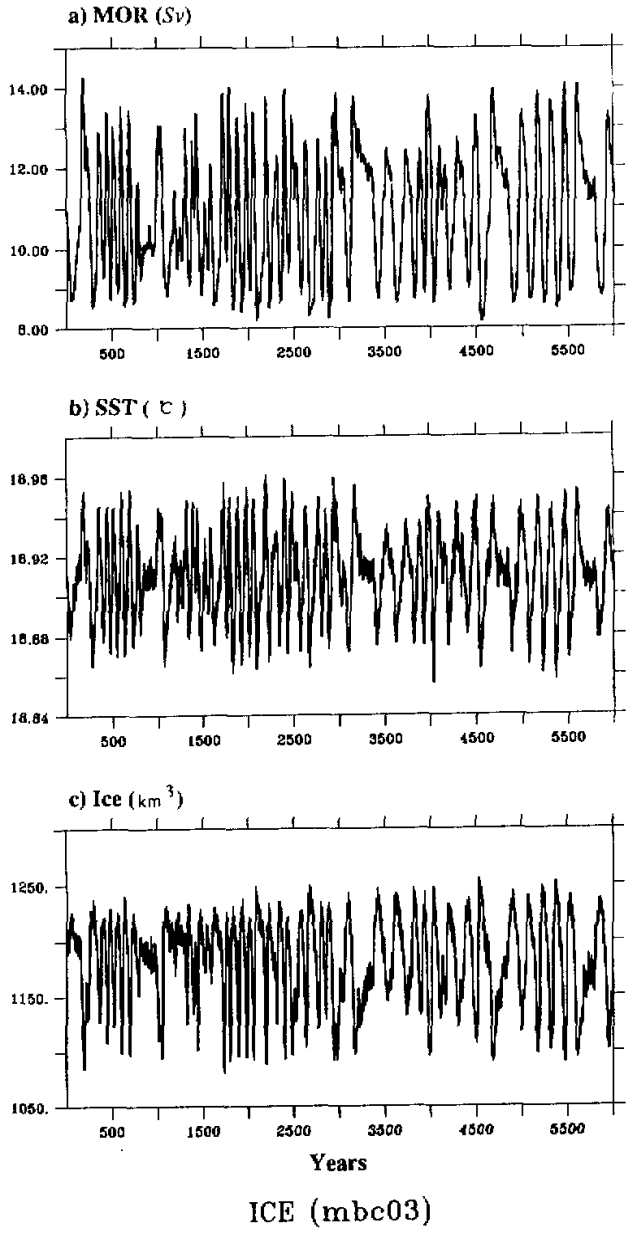

Fig. 2. Time series of the annual-mean (a) meridional overturning rate, (b) basin-mean sea surface temperature and (c) total ice volume.

stability of the solution is altered substantially. Consequently, models based on the relaxation condition for salinity are not suitable for climate variability study, and more realistic boundary conditions, such as the virtual salt flux condition or the natural boundary condition, should be used.

Thus, we use the quasi–equilibrium state reached under the relaxation conditions to diagnose the equivalent monthly–mean virtual salt flux from the final quasi–equilibrium state of the model. The model is then restarted from the quasi–equilibrium state and run under the mixed boundary condtions, i.e., a relaxation condition for temperature and a flux condition for salinity, for 6,000 years. Irregular centennial oscillations appeared (Fig. 2). The meridional overturning rate oscillates between maximum values of 13–14 Sv and minimum values of 8–9 Sv, while the amplitude of the basin–mean surface temperature and the total ice volume oscillate almost in phase with the meridional overturning rate. The basin–mean salinity also oscillated similarly (not included because the basin–mean salinity change is almost in phase with other model variables).

Note that the basin–mean surface temperature change is quite small, and this is due to the strong relaxation condition imposed on the temperature. This strong relaxation condition also contributes to the following two results. First, the basic state of the circulation is in the thermal mode, with deep water sinking at high latitudes. Second, the basic state of the thermal mode is quite stable, and the permissible temperature perturbations are relatively small. On the other hand, salinity is subject to a flux condition, so it has more freedom to fluctuate. As a result, the thermohaline oscillations in the system are primarily salinity controlled.

Spectral analysis of the annual–mean meridional overturning rate recorded over 6000 years indicates that the peak of the power spectrum is around 106 years (Fig. 3); while the power spectrum analysis over the first 3000 years indicated a peak around 86 years. The period of the irregular oscillations increases clearly over the last 3000 years. Thus, the period of oscillations in our model is about twice as much as the 50–year period in an ocean–atmosphere coupled model reported by Delworth et al. (1993). There are major differences between these two models: First, our model is a regional model for a single Northern Hemisphere basin. Second, our model is de–coupled from the atmosphere. Nevertheless, oscillations observed from these two models share many common features. Actually, one of the main conclusions from our study is that the centennial oscillations observed in the coupled model represent an oceanic oscillation mode, as speculated by Delworth et al.(1993). Thus, in the following analysis we will concentrate on the basic mechanism of the centennial oscillations observed in our model.

4. Discussion

As shown in Fig. 2 the centennial oscillations are irregular over a long period of model simulation. Within a short period, however, the oscillation appears to behave rather regularly, both in time and space. Such charactertistics are quite common in non–linear oscillations, reflecting partially the fact that the system is beyond the first Hopf bifurcation, and may enter the second or higher bifurcations (e.g., Huang and Dewar, 1996). The irregular oscillations are often the nonlinear resonances to the annual cycle in the forcing fields. The mechanism for the oscillations is likely to remain the same even when the periods change somewhat. To understand it we decided to examine the model's behavior in one particular oscillatory cycle, starting at year 2772 and ending at year 2851. The choice is rather arbitrary. We have compared this cycle's characteristics, including time evolution, spatial patterns, and

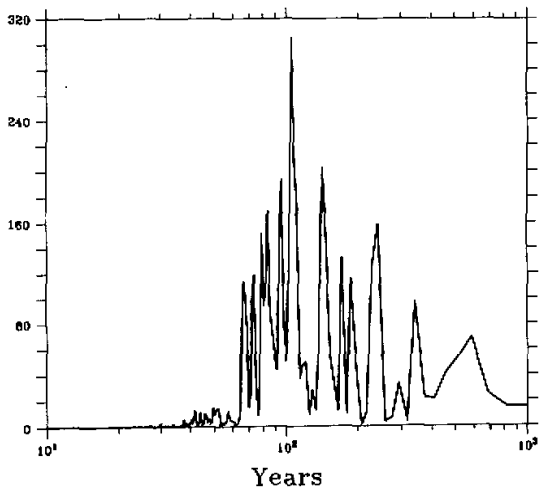

Fig. 3. Power specturm density.

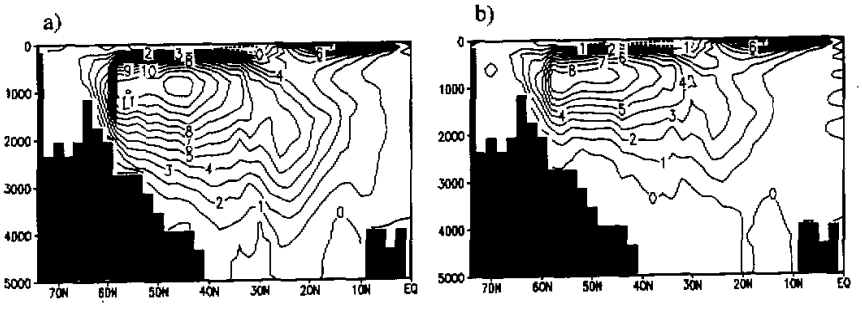

Fig. 4. Meridional overturning streamfunction maps at the phase of peak maximum (a) and minimum (b). Units are in Sv.

phase relations among variables, with some other cycles with different oscillation periods, and found that they resemble each other closely. So the oscillation mechanism discovered from this particular cycle is representative and can be applied to others. For simplicity, in the following analysis of this 80-year cycle, we will re-label the year 9017 as year 1.

At year 1, the annual-mean meridional overturning rate is about 12.8 Sv, and the overturning cell penetrated all the way to below 3 km (Fig. 4a). On the other hand, at year 37 the meridional overturning cell is much shallower, and the minimum overturning rate is only about 8.5 Sv (Fig. 4b). In general, thermohaline oscillations originate in the upper layer of the subpolar gyre, and manifest themselves mostly in the upper kilometer of the ocean. Nevertheless, the oscillations also affect the deep circulation profoundly, it will be shown shortly.

Similar to Delworth et al. (1993), we will examine the region of deep-water formation, which covers an area between 55°W–38°W and 40°N–58°N. The temporal evolution of the density anomaly and its components due to temperature and salinity clearly showed that the density anomaly at the site of deep water formation is dictated by the salinity anomaly. In addition, the density anomaly leads the overturning circulation by about 10 years (Fig. 5). Thus centennial oscillations in the model are primarily driven by the density anomaly due to salinity perturbations.

4.1 *The mechanism of oscillation*

Thermohaline oscillations can be driven by both the temperature and salinity variations, especially in the vicinity of the region of deep-water formation. Understanding processes attributable to density variations is a key toward understanding the mechanism for the oscillations. The temporal evolution of the model temperature and salinity is determined by diffusion, advection and convection. We shall analyze the dynamic role of each process and explore the interactions and competition between these processes.

a) Diffusion, both in vertical and horizontal, mainly acts to damp T and S anomalies, so it is a stabilizing process. Varying model diffusivity could modify the model flow regime, altering the stability or shifting the model's bifurcation points. This can lead to the changes of oscillation periods, and to more chaotic or more regular model behaviors. However, diffusion alone is unlikely to be responsible for generating the model oscillations.

b) Advection includes contributions from both overturning circulation and horizontal gyre circulation. The meridional overturning transports both salt and heat from low latitudes to the sinking region. A higher (lower) overturning rate makes surface water in the subpolar

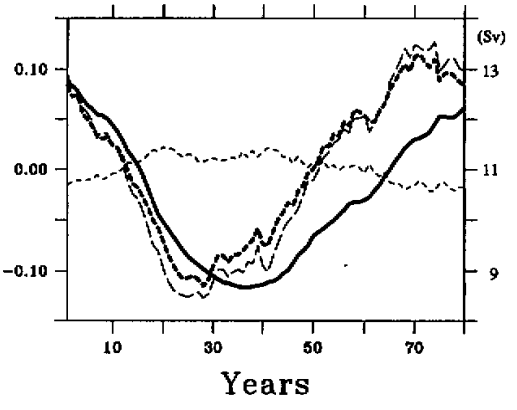

Fig. 5. Phase relation within a typical cycle from year 9017 to 9096. The time coordinate origin is set to year 9017. The solid curve is for the meridional overturning rate (in Sv), the heavy dashed curve is for the density anomaly (in σ), at the sinking site; the thin long dashed curve is for the density anomaly due to surface salinity; and the thin short dashed curve for the density anomaly due to surface temperature.

basin warmer (cooler) and saltier (fresher). The changes in temperature and salinity are associated with two opposite types of feedbacks to the overturning circulation—a negative feedback of temperature and a positive feedback of salinity. The competition between these two distinct types of feedbacks is the basic mechanism controlling the thermohaline oscillations.

The feedback loop of temperature is as follows. An initial negative temperature anomaly accelerates the meridional overturning cell, resulting in more poleward heat transport and warming of the subpolar ocean. This in turn tends to weaken the overturning cell and to reverse the temperature anomaly. Due to the inertia of the meridional overturning cell, this temperature reversion may overshoot, thus this feedback does contain a potential mechanism for oscillations. Because of the strong relaxation condition on sea surface temperature, such thermal oscillations are stable and their amplitude is small, if there is no additional destabilizing processes.

On the other hand, the salinity / overturning feedback is positive. For example, an initial positive salinity anomaly in the deep–water formation area strengthens the overturning, and leads to more poleward transport of salt and a growth of the initial positive density anomaly. This instability mechanism, when coupled with stabilizing feedback mechanisms of the temperature / overturning, might sustain a finite amplitude oscillation. In our model, the surface temperature anomaly is strongly damped due to the negative feedback between the SST and heat flux, and thus, the surface density anomaly due to the temperature changes is relatively small. Salinity, however, is subject to a flux condition, so it can vary more freely. Due to the positive feedback mechanism discussed above, the salinity perturbation, parasitic on an existing thermal mode, is dynamically unstable (e.g., Walin, 1985; Marotzke, 1989). In the following discussion, we will examine the details of how the growth of the surface salinity anomaly is arrested and reversed during the time of peak meridional overturning rate.

Oscillations in three–dimensional models also involve horizontal gyres. The gyre circulation can either intensify or weaken density anomalies in the subpolar region depending on the along–stream density gradients. To explore this process we plotted the sea surface temperature, salinity, and current anomalies at four consecutive phases during an oscillatory cycle, starting at the maximum overturning state (the first row in Fig. 6).

At the peak of the meridional overturning phase (the first row in Fig. 6), the subpolar basin is generally warm and salty, while cold, fresh water appears in the south off Newfoundland. This structure bears some similarities to observed anomalies reported by Deser and Blackmon (1993) and Kushnir (1994), and to model results obtained by Delworth et al. (1993). Associated with this maximum overturning state, there is a strong northward current originating from the Gulf Stream extension and extending all the way to the sinking region. This anomalous current feeds the subpolar basin, where it converges near the southern tip of Greenland and produces an anomalously high volume of deep water at this phase.

This scenario is generally consistent with the results of Delworth et al. (1993). In comparison with their model, the positive SST and SSS anomalies in the subpolar basin, however, are divided into two poles, one to the northwest and the other to the southeast of the model's deep–water formation region. To answer the question of why both the SST and SSS anomalies start to decline at the time when the meridional overturning rate is maximum, we need to examine the salinity advection at the peak of the meridional overturning rate by plotting the anomalous SSS and mean surface currents (Fig. 7a) and the mean SSS and anomalous currents (Fig. 7b).

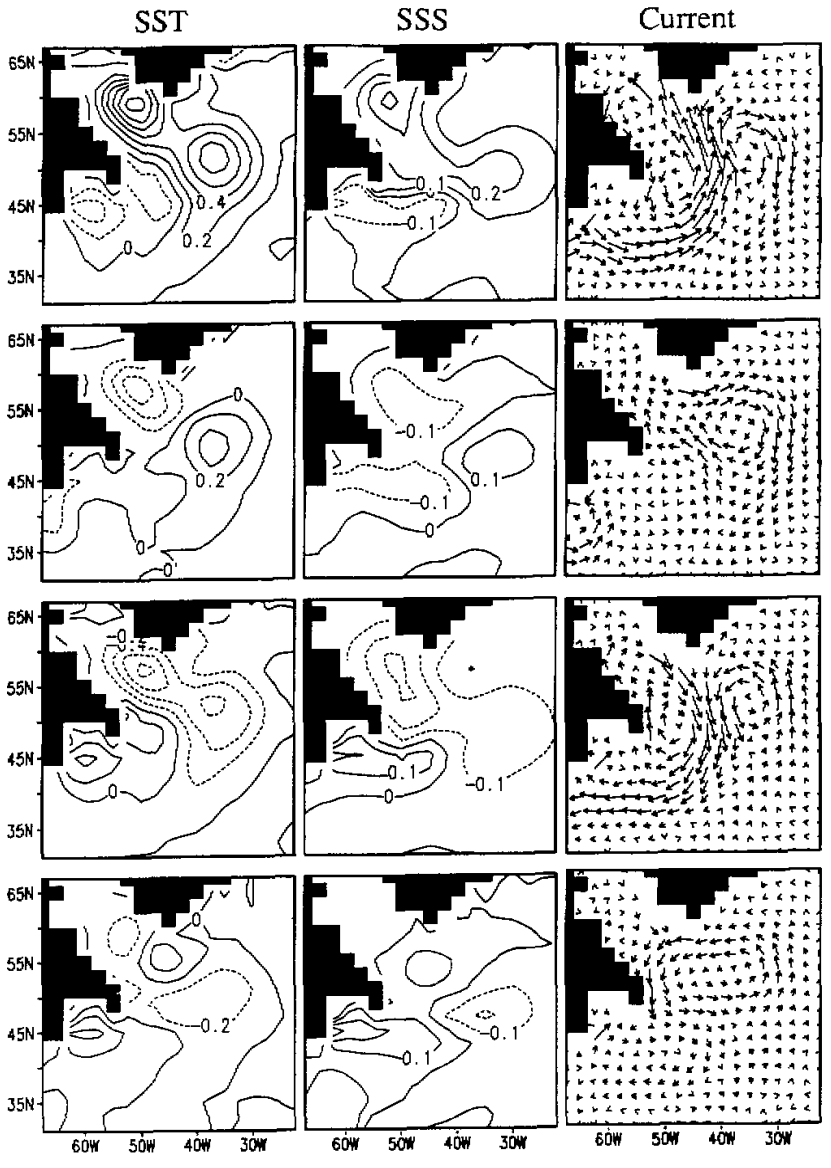

Fig. 6. Composite patterns of surface temperature anomaly, surface salinity anomaly, and surface current. The top row corresponds to the phase of maximum meridional overturning rate, the second row is 1 / 4 period, the third row 1 / 2 period, and the third row 3 / 4 period.

The salinity anomaly due to advection consists of two terms, i.e., $\vec{u}' \cdot S'$ and $\vec{u}'\overline{S}$. The first term is due to salinity perturbation advected by the mean current, and the second term is due to the mean salinity advected by the velocity perturbation. During the meridional

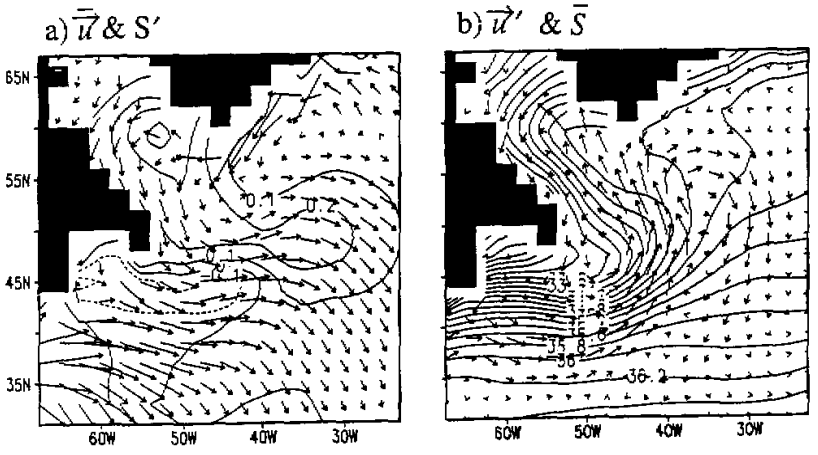

Fig. 7. Salinity advection due to (a) salinity anomaly advection by the mean velocity, and (b) mean salinity advection by the velocity perturbation.

overturning maximum, a strong mean current off Greenland carries the fresh anomaly southwestward into the site of deep water formation (Fig. 7a). In addition, there is a "fresh tongue" off Newfoundland (Fig. 7b) in the mean salinity field. So the meridional gradient of the mean salinity between 45°N and 60°N within a zonal band between 55°W and 40°W is positive. Within this region, the northward velocity anomaly actually brings low salinity water from the "fresh tongue" off Newfoundland to the sinking region. Thus, both terms in the anomalous salinity advection work together to bring down the salinity in the sinking region.

Similarly, temperature advection also brings cold water into the site of deep water formation, thus creating a "cold tongue". However, the northward gradient of the mean SST near the site of deep water formation is rather weak (Fig. 1a), and hence, the heat advection due to the advection of the mean temperature by the anomalous northward current is less effective in the sinking region. In addition, the southwestward East Green-land Current in the mean state (Fig. 7b) also brings anomalously colder water to the deep-water formation region. The temperature is subject to a strong relaxation boundary condition, thus the amplitude of the SST anomaly is rather limited.

Therefore, at the time of meridional overturning maximum, both surface salinity and temperature in the sinking region start to decrease due to the horizontal advection. Since the salinity anomaly is subject to a flux condition, it is unconstrained by the surface flux. As a result, the salinity anomaly has an amplitude much larger than that of temperature, and the density anomaly is dictated by the salinity anomaly. The decline of density at the site of deep water formation in turn decelerates the overturning rate. It is important to note that the declines of both SSS and SST actually start even before the meridional overturning rate reaches its maximum, as shown in Fig. 5, thus, the salinity anomaly is the driving force for the oscillations.

At about one quarter cycle after the overturning maximum, both temperature and salinity have decreased and the negative anomalies start to appear in the region of deep-water

formation (the second row in Fig. 6). In the meantime, the anticyclonic gyre associated with the warm and salty pole to the southeast of the sinking region remains. It transports fresh and cold water to the eastern side of the sinking region. Thus, this gyre further intensifies the cold and fresh anomalies. At half of the cycle, the overturning reaches its minimum, and the salinity and temperature advection goes in the direction opposite to that at the beginning of the cycle, thus salinity and temperature in the sinking region start to increase. Note that the specific cycle we have chosen is not a perfect periodic cycle, so the pattern at 1 / 2 of the cycle is not exactly opposite to that at the beginning of the cycle. The difference is, however, small, and the diagnosis of this cycle is useful to our understanding of the oscillations.

c) The convection in the site of deep water formation can bring the warmer and saltier deep water up to the surface, thus creating positive temperature and salinity anomalies. Because of the mixed boundary condition, the positive SST anomaly due to the convection would be rapidly cooled, while a positive salinity anomaly is sustained. This leads to further densification of the surface water, and to more vigorous convection. Thus, the convective process is a positive feedback and plays a destabilizing role.

As shown in Fig. 8, the density anomaly in the whole water column is positive during the time of maximum meridional overturning rate, thus, more convection occurs. This results in warmer and saltier surface layer in the upper 500 meters, and cooler and fresher deep water.

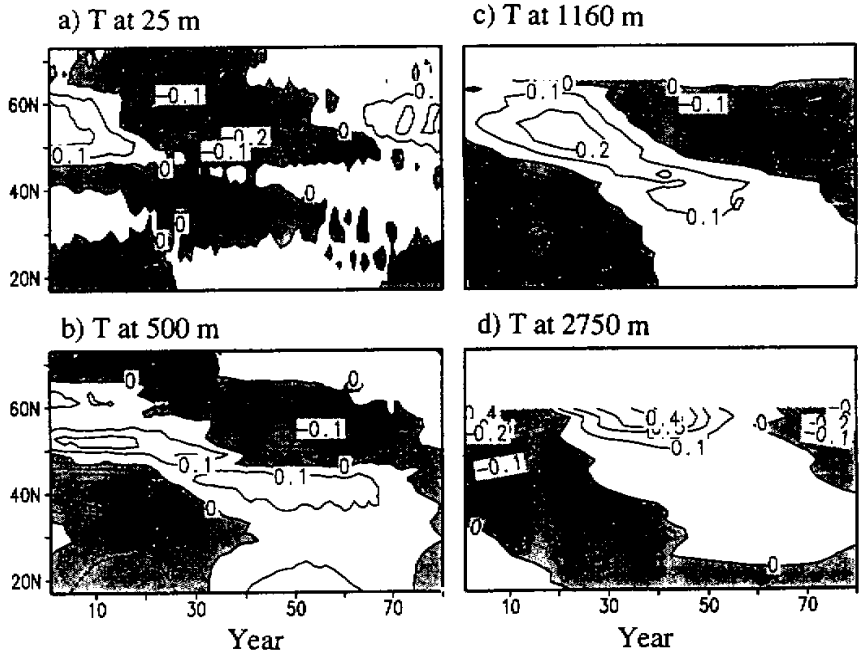

Fig. 8. Time series of (a) density anomaly (in σ), (b) temperature anomaly in (°C), and (c) salinity anomaly (in psu) at a station southwest of the tip of Greenland. Note the different vertical scale and contour level used for the upper 500 meters.

Due to the advective processes described above, both temperature and salinity decrease. Note the rapid changes in the temperature and salinity anomaly at about year 18. The rapid change in the surface temperature is apparently due to the advection of cold water and a sudden change in the strength of the convection. Because of the cold and fresh advection, the surface water density at the site of deep water formation rapidly declines to a critical level, so the advection is basically switched off, or of very weak intensity. The slow convection combining with advective processes produces cold, fresh surface water in the subpolar basin. Similar to the case at the time when the meridional overturning rate is at its maximum, the density anomaly is dictated by the contribution due to the salinity anomaly. Thus, the density of sea water at the site of deep water formation declines, so the meridional overturning is low.

We have described the potential contributions to the oscillations from diffusion, advection, and convection. Now we will examine how these processes work together to generate such an oscillation. At the stage of maximum overturning rate, the surface subpolar ocean is warm and salty due to the heat and salt transported by the anomalous meridional overturning cell. The strong southwestward current south of Greenland brings the fresh anomaly from the northeastern subpolar basin to the site of deep water formation (Fig. 7a). In addition, the anomalous northward current brings fresh water from the "fresh tongue" (in the mean salinity field) to the deep-water formation area (Fig. 7b). Thus, both perturbation terms in the salinity balance work together and lead to freshening and less convection in the sinking region.

The weaker convection cuts down the heat and salt flux brought from the deep ocean, so the surface layer becomes even cooler and fresher (Fig.8). The surface density declines because the surface temperature is strongly controlled by the relaxation constraint, but the surface salinity can be altered much more freely. As a result, the overturning cell slows down. The anomalous northward current disappears after the overturning weakens. But a high density pole to the southeast of the sinking region is sustained longer because it is less affected by the convective feedback and the fresh tongue advection (row 2 in Fig. 6). An anticyclonic gyre associated with this high density pole advects cold and fresh water eastward. But its contribution to the freshening in the sinking region is probably smaller since this gyre is located a bit away from the sinking region. So the convection feedback is likely to play a leading role in freshening.

The overturning circulation reaches its minimum due to the freshwater cap. A southward anomalous current develops, flushing fresh water away from the sinking region, and advects warmer and saltier water into the sinking region (row 3 in Fig. 6). This leads to more convection (Fig. 8) which in turn brings warm and salty deep waters to the surface. The overturning is then accelerated. A cyclonic gyre develops between the minimum and maximum overturning states (row 4 in Fig. 6). It brings warm and salty water westward to the sinking region in the same way as Delworth et al. (1993) described in their model. The mechanism we discuss here bears some similarities to that discussed by Delworth et al. (1993), but includes additional important contributions from the "fresh tongue" advection and the positive convection feedbacks.

4.2 *The spatial propagation of the anomaly*

The signals of the temperature and salinity oscillations are originated in the surface layer within the region of deep-water formation. Such signals may be transmitted away from their source to other parts of the basin, primarily via the deep western boundary current. Figs. 9 and 10 show the latitude vs time plots of the zonally averaged temperature and salinity at 4

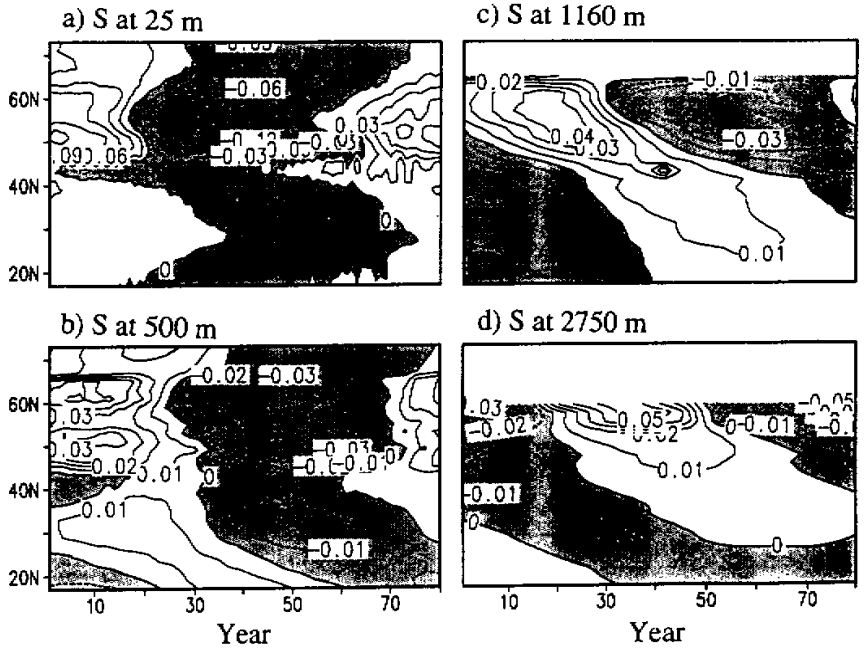

Fig. 9. Horizontal propagation of temperature anomaly at different levels.

different depths. Near the surface at 25 m depth the oscillation is largely localized in the subpolar basin (Fig. 9a and Fig. 10a), exhibiting a standing wave pattern. At greater depths, there are clear signals of southward propagation especially below 1000 meters.

The time series of anomalous temperature and salinity taken at a station near Bermuda at 31°N, 65°W are shown in Fig. 11. By comparing with Fig. 8, it indicates that it takes about 10 to 15 years for the anomalous cold, fresh water (with anomalies of about −0.1°C and −0.02 psu in both Fig. 8 and Fig. 11) to travel from the sinking region to Bermuda. This is considerably longer than the 5–7 years recently reported by Curry and McCartney (1996). The slower propagation speed in our model is probably due to the low resolution used. The slow propagation speed of the anomaly may affect the basin–wide response of the oscillations. Thus, it is quite possible that oscillation periods may be sensitive to the resolution of the model.

In contrast to the subpolar ocean, density perturbations in the subtropical basin are controlled by temperature rather than salinity anomalies. This is due to the nonlinearity of the equation of state whose sensitivity to temperature variations increases with warmer waters. This is shown in Fig. 12, in which we plotted the time series of (a) the density anomaly, (b) the temperature anomaly, and (c) the salinity anomaly along a zonal cross–section at 21°N.

4.3 *The role of the seasonal cycle*

The model includes the full seasonal cycle in all forcing fields. In addition to the low–frequency variations, the model also exhibits the seasonal cycle clearly. Figure 13 shows the SST

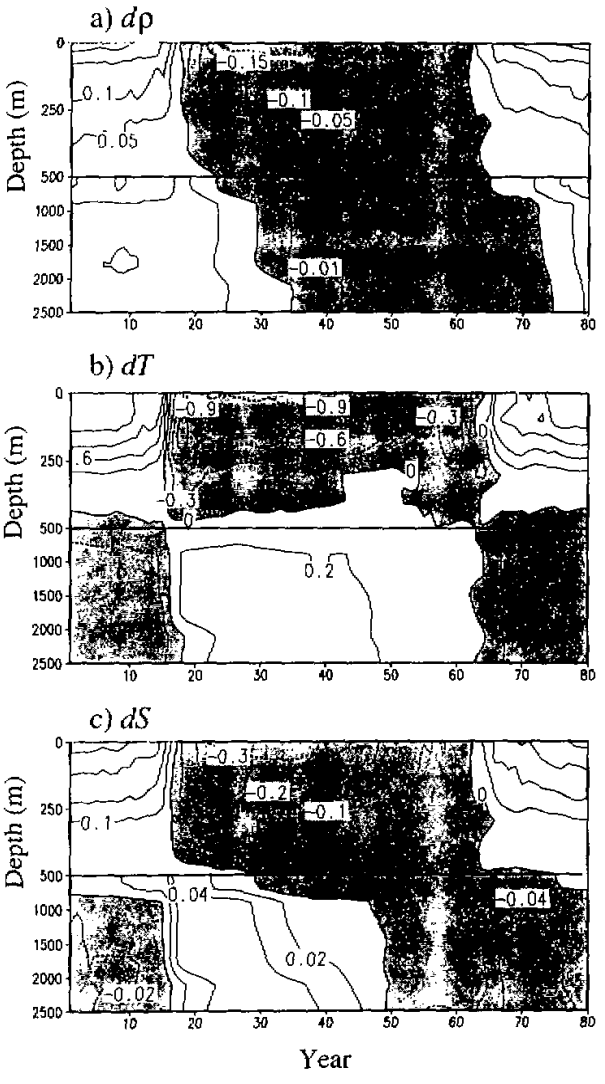

Fig. 10. Horizontal propagation of salinity anomaly at different levels.

and SSS in the sinking region over one centennial oscillation cycle. It is interesting to note that the amplitude of seasonal variation of the SST is much greater when the overturning is weak, but the amplitude of the seasonal cycle in SSS is small during the overturning rate minimum. The minimum SST in the winter reaches as low as the freezing point of −2°C between 20th and 60th years when the overturning rate is low while it can be as high as 1°C when the overturning is strong.

The SST is primarily controlled by advection, surface flux, and convection, while diffusion plays a minor role. During the stage of weak overturning rate, both northward heat

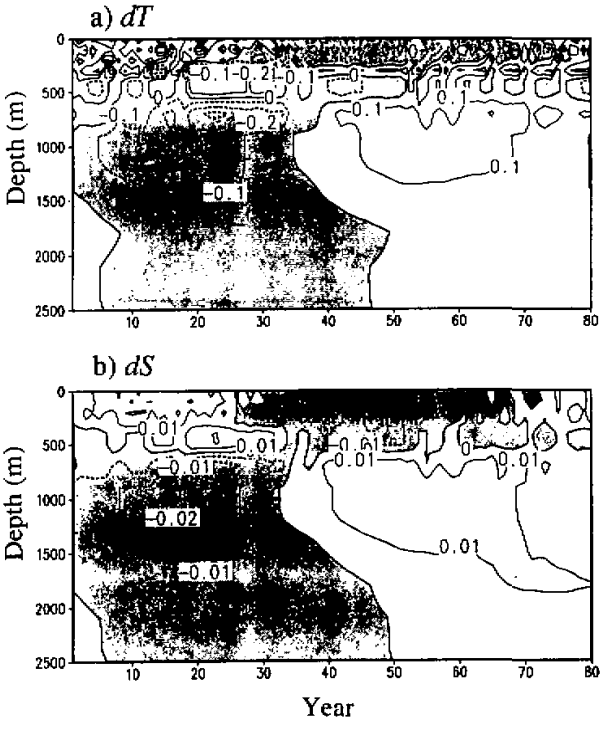

Fig. 11. Time series of (a) temperature anomaly (in °C) and (b) salinity anomaly (in psu) at a station near Bermuda.

advection and upward heat flux by convection are dramatically reduced. Thus, due to the large heat loss to the atmosphere, the water temperature is cooled to near the freezing point. When the overturning is strong, the northward heat flux to the sinking region is enhanced and more vigorous convection mixes the warm deep water to the surface. Given a similar amount of heat loss to the atmosphere, the additional heat gain will maintain the temperature substantially above the freezing point. The seasonal variation of salinity is slightly smaller than the SST. The salinity increases toward winter and decreases toward summer. When the overturning is strong, the local convection brings up salty deep water to the surface and then further enhances the seasonal increase of the salinity. That explains partially why the seasonal variation of the SSS is greater when the overturning is strong.

To examine the role of the seasonal cycle in the oscillation mechanism, we have run an additional experiment in which the seasonal cycle is removed using the annual mean wind stress, surface salinity flux, and the annual mean Haney condition for the heat flux. We first spun up the model by relaxing the SSS toward its annual mean climatology to an equilibrium state, and then diagnosed the virtual salt flux for this equilibrium state. The model is then restarted by switching to the mixed boundary condition. The procedure is the same as that described in Section 2, except for using the annual mean forcing fields. Unlike the previous case, however, the model is now stable under the mixed boundary condition. The initial

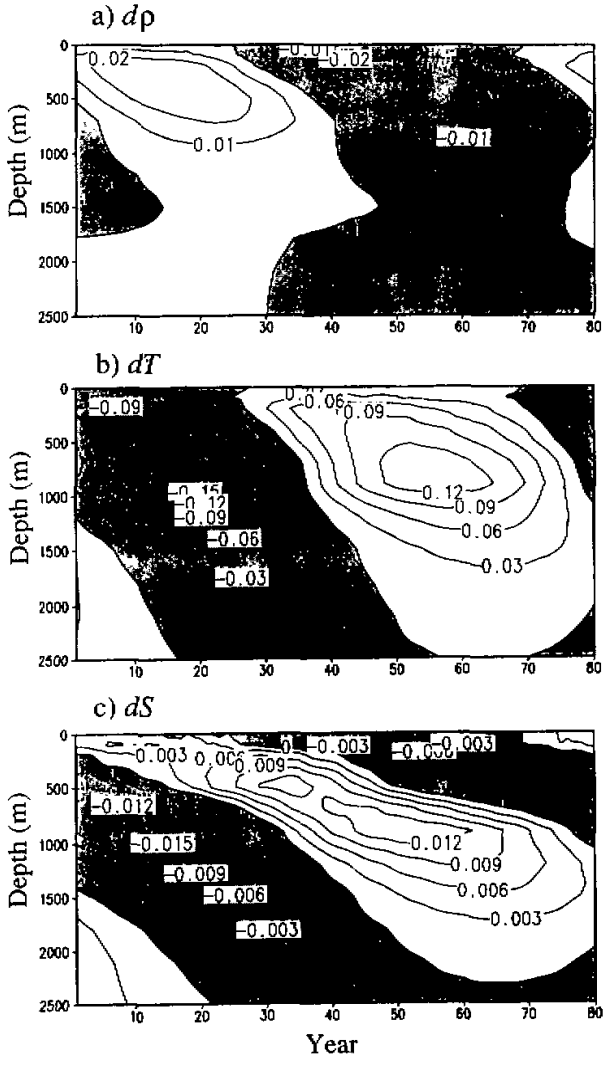

Fig. 12. Time series of (a) density anomaly (in σ), (b) temperature anomaly (in °C), and (c) salinity anomaly (in psu) along a zonal cross-section at 21°N.

perturbations induced by switching the boundary condition decayed rapidly, and the model ocean returned to the same equilibrium state. Thus, for the parameter regime examined here, a model without the seasonal cycle in the forcing fields cannot sustain oscillations.

The previous studies indicated that the seasonal cycle can play an active role in low-frequency oscillations. Yang and Huang (1996) have identified a subharmonic oscillation with a 14-year period in a two-dimensional coupled ocean-ice model. The annual cycle may also modify the model flow regime, or shift the model bifurcation points, resulting in a

non–oscillatory state. These are complicated processes and it is very difficult to sort out all the cause–and–effect processes involving the seasonal cycle. Further study is then needed.

However, there is one aspect of the seasonal cycle that was identified and believed to play an important role in the oscillation. As discussed earlier by us, during the weak overturning phase the minimum water SST in the sinking region is about 3°C colder than that during the strong overturning phase. Convection is reduced, and even partially shut off, mostly due to the low surface salinity. Since SST in winter is now much lower, convection may still occur for a short period at the peak of winter. If that happens, it brings up salty water to the surface, and helps to arrest the declining trend of the surface salinity associated with weakening overturning.

In fact, the SSS starts to rebound at about the 25th year (Fig. 13b) when the overturning is still weakening. In the annual mean case, however, the SST in the sinking region would be in the range of about 1°C, e.g., an average between maximum summer SST and minimum

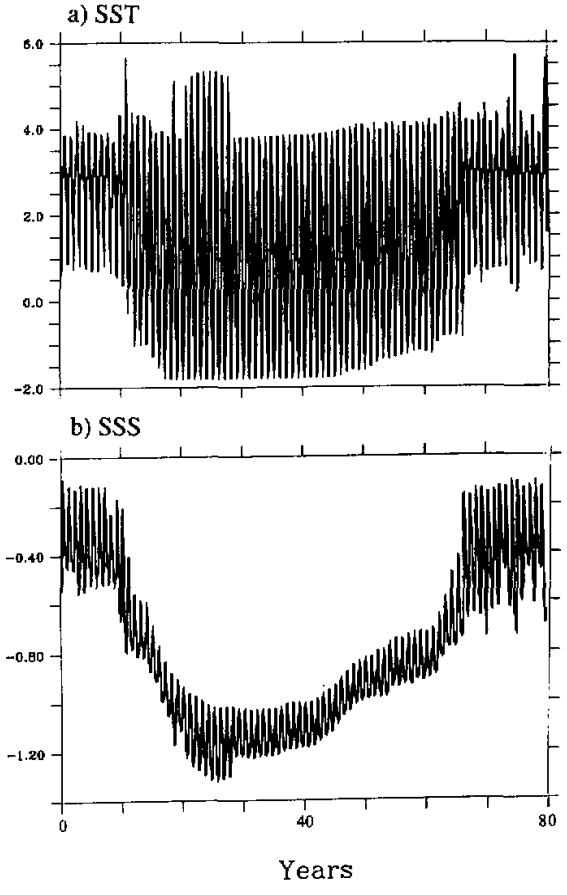

Fig. 13. Seasonal cycle of temperature (in °C) and salinity anomaly (in psu) at a station southwest of the tip of Greenland.

winter SST in Fig. 13a. This annual averaged value will not make the surface water sufficiently dense to sink and mix with the deep water when the thermohaline circulation is weak. In that case, the salinity will continue to decline with overturning, and might stay in a steady state of weak overturning with low SSS in the sinking region if other processes alone are not strong enough to turn it around. Therefore, the winter convection associated with the seasonal cycle contributes to sustain the oscillations.

4.4 *Sea–ice interaction*

The model includes active interaction with sea ice. Sea ice may affect the meridional overturning in two ways; through brine rejection (e.g., Yang and Neelin, 1993; Yang and Huang, 1996), or through its thermal insulation (e.g., Yang and Neelin, 1997). To examine the possible role of sea ice, we carried out two additional experiments. First, we removed the brine rejection term in the surface salinity flux and restarted the model exactly as we did in the standard run. The model behavior, including the periods and amplitudes of the oscillations, remained virtually unchanged. Thus, the freshwater flux associated with freezing and melting does not play an essential role in setting the oscillations in the model. This is not in contradiction with the previous studies (e.g., Yang and Huang, 1996) which emphasize the decadal time scales. For shorter time scales, the melting rate from maximum ice cover to minimum ice cover over a half cycle, say 5 to 7 years, is compatible with the net precipitation / evaporation in the subpolar basin. For centennial time scales, such freshwater flux rate is one order of magnitude smaller and therefore negligible.

In the second experiment, the ice edge was fixed at its mean position over an oscillatory cycle. Again the model's solution changed only slightly, in comparison with the standard case. This is understandable because the sea–ice extent affects only the shelf regions along the boundary, while the site of deep–water formation is mostly ice free (Fig. 1a). However, our study does not exclude the possibility that sea ice may have a greater effect at higher latitudes, such as in the Greenland Sea and the Arctic Ocean which are excluded from our model.

5. Conclusion

Using an ocean–ice coupled model with realistic geometry and seasonal forcing to simulate the circulation in the North Atlantic, we have found that the model exhibits irregular centennial oscillations, with a spectrum peak at 106 years. The oscillation mechanism involves the interplay between heat and freshwater transports by the meridional overturning cell, gyre circulation especially the advection of low salinity waters from the "fresh tongue", and convection. The seasonal cycle plays an important role in the oscillations, and the centennial oscillations disappear if the model is forced by the annual mean. The near freezing SST in the winter during the weak overturning phase may trigger some spontaneous convection that helps to turn around the salinity decline and thus to sustain the oscillation. For the centennial oscillations, sea ice plays only a minor role.

The period observed in our model is about twice as much as the 50–year period reported by Delworth et al. (1993) for the oscillations in the North Atlantic, obtained from a global ocean–atmosphere coupled model. The driving mechanism also bears some similarities regarding the advection by overturning and gyre circulation in some phases. But additional processes, like "fresh tongue" advection, convection, and the seasonal cycle, also play important roles in our model. Nevertheless, our diagnostic study confirmed their hypothesis that the oscillations at the time scales of multiple decades are driven by the oceanic processes alone.

Huang R.X. and Jin X.Z. were supported through the NASA grant NAGW-4331 and the NSF grant OCE93-00706. Yang J.Y. was supported through the NOAA grant NA56GP0209.

REFERENCES

Curry, R. G., and M. S. McCartney, 1996: Subtropical response to subpolar convection variability, manuscript.

Delworth, T. L., 1996: North Atlantic interannual variability in a coupled ocean-atmosphere model. *J. Climate*, **9**, 2356-2375.

Delworth, T., S. Manabe, and R. J. Stouffer, 1993: Interdecadal variatoins of the thermohaline circulation in a coupled ocean-atmosphere model. *J. Climate*, **6**, 1993-2011.

Deser, C., and M. L. Blackmon, 1993: Surface climate variations over the North Atlantic during winter: 1900-1989. *J. Climate*, **6**, 1743-1753.

Haney, R. L., 1971: Surface thermal boundary condition for ocean circulation models. *J. Phys. Oceanogr.*, **1**, 241-248.

Hellerman, S., and M. Rosenstein, 1983: Normal monthly wind stress over the world ocean with error estimates. *J. Phys. Oceanogr.* **13**, 1093-1104.

Huang, R. X., and W. Dewar, 1996: Haline circulation in a loop model. *J. Phys. Oceanogr.*, **26**, 2093-2106.

Kushnir, Y., 1994: Interdecadal variations in North Atlantic sea surface temperature and associated atmospheric conditions. *J. Climate*, **7**, 141-157.

Levitus, S. 1994: World Ocean Atlas 1994: CD-ROM Data Set Documentation, NODC, Informal Report No. 13, 30pp.

Marotzke, J., 1989: Instabilities and multiple steady states of the thermohaline circulation. In: Oceanic Circulation Models: Combining Data and Dynamics, D. L. T. Anderson and J. Willebrand, eds., NATO ASI series, Kluwer, 501-511.

Pacanowsky, R. C., 1995: MOM2 documentation user's guide and reference manual, version 2, GFDL Ocean Technical Report #3.

Parkinson, C. L., and W. M. Washington, 1979: A large-scale numerical model of sea ice. *J. Geophys. Res.*, **84**, 311-337.

Trenberth, K. E., 1992: Global Analyses from ECMWF and Atlas of 1000 to 10 mb Circulation Statistics. Tech. Rep. NCAR / TN-373+STR, National Center for Atmospheric Research, Boulder, Colorado.

Tziperman, E., J. R. Toggweller, Y. Feliks, and K. Bryan, 1994: Instability of the thermohaline circulation with respect to mixed boundary conditions: is it really a problem for realistic models? *J. Phys. Oceanogr.*, **24**, 217-232.

Walin, G., 1985: The thermohaline circulation and the control of the ice age. *Palaeogeogr., Palaeoclimatol., Palaeoecol.*, **50**, 323-332.

Yang, J., and R. X. Huang, 1996: Decadal oscillations driven by the annual cycle in a zonal-averaged coupled ocean-ice model. *Geophys. Res. Lett.*, **23**, 269-272.

Yang, J., and J. D. Neelin, 1993: Sea-ice interaction with the thermohaline circulation. *Geophys. Res. Lett.*, **20**, 217-220.

Yang, J., and D. J. Neelin, 1997: Sea-ice interaction and the stability of the thermohaline circulation. *Atmos. Ocean*, 433-469, V35.